

Photoluminescence of green nanophosphors $Sr_2MgSi_2O_7$ doped with Tb^{3+} under 374-nm excitation

Bo-Shi Mu(牟博石), Yi Zhang(张熠), Qing-Feng Bian(边庆丰), Cheng-Ren Li(李成仁), Zhi-Chao Li(李志超), Yun-Ting Chu(褚云婷), Feng Zhao(赵峰), and Jing-Chang Sun(孙景昌)

Citation: Chin. Phys. B, 2021, 30 (**12**): 123201. DOI: 10.1088/1674-1056/abfbce
Journal homepage: http://cpb.iphy.ac.cn; http://iopscience.iop.org/cpb

What follows is a list of articles you may be interested in

Comparisons of electrical and optical properties between graphene and silicene-A review

Wirth-Lima A J, Silva M G, Sombra A S B
Chin. Phys. B, 2018, 27 (**2**): 023201. DOI: 10.1088/1674-1056/27/2/023201

Field ionization process of Eu $4f^7 6snp$ Rydberg states

Zhang Jing, Shen Li, Dai Chang-Jian
Chin. Phys. B, 2015, 24 (**11**): 113201. DOI: 10.1088/1674-1056/24/11/113201

Precision frequency measurement of $^1S_0$-$^3P_1$ intercombination lines of Sr isotopes

Liu Hui, Gao Feng, Wang Ye-Bing, Tian Xiao, Ren Jie, Lu Ben-Quan, Xu Qin-Fang, Xie Yu-Lin, Chang Hong
Chin. Phys. B, 2015, 24 (**1**): 013201. DOI: 10.1088/1674-1056/24/1/013201

Spectral decomposition at complex laser polarization configuration

Yang Hai-Feng, Gao Wei, Cheng Hong, Liu Hong-Ping
Chin. Phys. B, 2013, 22 (**5**): 053201. DOI: 10.1088/1674-1056/22/5/053201

Exact quantum defect theory approach for lithium in magnetic fields

Xu Jia-Kun, Chen Hai-Qing, Liu Hong-Ping
Chin. Phys. B, 2013, 22 (**1**): 013204. DOI: 10.1088/1674-1056/22/1/013204

Photoluminescence of green nanophosphors $Sr_2MgSi_2O_7$ doped with Tb^{3+} under 374-nm excitation*

Bo-Shi Mu(牟博石)[1,2], Yi Zhang(张熠)[1], Qing-Feng Bian(边庆丰)[1], Cheng-Ren Li(李成仁)[1,†], Zhi-Chao Li(李志超)[1], Yun-Ting Chu(褚云婷)[1], Feng Zhao(赵峰)[1], and Jing-Chang Sun(孙景昌)[1]

[1] *School of Physics and Electronic Technology, Liaoning Normal University, Dalian* 116029, *China*
[2] *School of Science, Qiqihar University, Qiqihar* 161006, *China*

(Received 6 March 2021; revised manuscript received 19 April 2021; accepted manuscript online 27 April 2021)

A series of $Sr_2MgSi_2O_7$:Tb^{3+} nanophosphors is prepared using a high-temperature solid-state reaction. The x-ray diffraction patterns show that the crystal structure of the sample is not significantly affected by Tb^{3+} ions. However, the images of the scanning electron microscope illustrate that the average size of nanoparticles becomes larger with the increase of Tb^{3+} concentration. Unlike earlier investigations on down-conversion emission of Tb^{3+} ion excited by deep ultraviolet light, in this work, the photoluminescence characteristics of $Sr_2MgSi_2O_7$ nanophosphors doped with different Tb^{3+} concentrations are analyzed under 374-nm excitations. The intense green emission at 545 nm is observed at an optimal doping concentration of 1.6 mol%. The main reason for the concentration quenching is due to the electric dipole–electric dipole interaction among Tb^{3+} ions.

Keywords: $Sr_2MgSi_2O_7$:Tb^{3+} nanophosphor, green emission, 374-nm excitation, electric dipole–electric dipole interaction

PACS: 32.30.Jc, 61.82.Rx **DOI:** 10.1088/1674-1056/abfbce

1. Introduction

The electrons occupied in outer shell of trivalent terbium ion is $4f^8 5s^2 5p^6$ electrons, and thus the spectrum produced by f–f transition of Tb^{3+} ion is a sort of atom-like spectrum due to the shielding effect of double closed shells $5s^2 5p^6$. In addition, Tb^{3+} ion also has abundant energy levels and a broad emission range from ultraviolet to infrared because of the large orbital angular momentum $l = 3$. Therefore, trivalent terbium ion is an excellent down-conversion active ion and attracts more and more attention.[1–6] For example, dos Santos *et al.* prepared Tb^{3+}-doped low silica calcium aluminosilicate glasses and analyzed their luminescence properties;[7] Gao *et al.* synthesized Zn_2GeO_4:Tb^{3+} nanophosphors and studied their photoluminescence (PL) characteristics under a deep ultraviolet (DUV) excitation at 265 nm.[8] In particular, they also discussed the energy transfer mechanism from Zn_2GeO_4 host to Tb^{3+} ion. Although some existing matrix materials, for instance, $KSr(Cd,Y)(PO_4)_2$,[9] $Ca_3Al_2Si_6O_{18}$,[10,11] BiOCl,[12] Y_2O_3,[13–16] MgAl-NO_3,[17] β-PbF_2 glass-ceramics,[18] Ba_2SiO_4,[19,20] *etc*, are all excellent hosts for Tb^{3+} ion, their optimal excitation wavelengths are in the deep ultraviolet (200 nm–280 nm) region. As is well known, the semiconductor chips in DUV region are very expensive, which is undoubtedly unconducive to wider applications of nanophosphor-doped Tb^{3+} ion in the field of light-emitting diode (LED) illumination. So it is important to explore some new host materials used to dope Tb^{3+} ion in order to extend the excitation wavelength toward a long wavelength. The $Sr_2MgSi_2O_7$ is of a typical pyrosilicate crystal structure belonging to the tetragonal system, especially it has stable chemical and physical properties and lower phonon energy. Therefore, $Sr_2MgSi_2O_7$ has attracted more and more interest and attention in recent years.[21–24] For example, Tshabalala *et al.* synthesized $Sr_2MgSi_2O_7$:Tb^{3+}, Eu^{3+} co-doped phosphor and realized simultaneously the blue and green emissions from Tb^{3+} ions and the red emission from Eu^{3+} ions, eventually resulting in the white emission;[25] Sahu prepared $Sr_2MgSi_2O_7$:Dy^{3+} and $Sr_2MgSi_2O_7$:Dy^{3+}, R (R = Li, Na and K) and observed near white light emission, moreover, the PL intensity was obviously enhanced through incorporating alkali metal as charge compensator ions.[26] Wang *et al.* synthesized $Sr_2MgSi_2O_7$:Ce^{3+}, Tb^{3+} and proved that the phosphor is promising candidate for WLED.[27] Most of previous researches choosing $Sr_2MgSi_2O_7$ as hosts, however, focused mainly on the long afterglow luminescence materials.[28–30] Few researches were involved with the investigating PL characteristics of $Sr_2MgSi_2O_7$:Tb^{3+} nanophosphor, particularly under a longer wavelength excitation.

In this work, we prepare a series of $Sr_2MgSi_2O_7$:Tb^{3+} nanophosphors through using the high-temperature solid-state reaction. The crystal structures and morphologies of representative samples are analyzed by x-ray diffraction (XRD) and scanning electron microscope (SEM). The results show that

*Project supported by the National Natural Science Foundation of China (Grant No. 11004092) and the Foundation of Science and Technology Department of Liaoning Province, China (Grant No. 201602455).

†Corresponding author. E-mail: lnnulicr@aliyun.com

© 2021 Chinese Physical Society and IOP Publishing Ltd

the crystal structure is not significantly affected by Tb^{3+} ions. However, the average size of nanoparticles becomes larger with the increase of Tb^{3+} concentration. The intense green emission at 545 nm is observed under a near ultraviolet (NUV) excitation at 374 nm, indicating that the price of semiconductor chips used for pumping can be significantly lowered once the excitation wavelength is selected in NUV region instead in DUV region. The PL characteristics of $Sr_2MgSi_2O_7$ nanophosphors doped under different Tb^{3+} concentrations are investigated and the optimal concentration is 1.6 mol%. The mechanism of concentration quenching is analyzed and driven mainly by the electric dipole–electric dipole interaction. It is predictable that $Sr_2MgSi_2O_7$:Tb^{3+} nanophosphor can play a more important role in fields of special lighting, WLED, and so on.

2. Experimental details

A series of $Sr_2MgSi_2O_7$:Tb^{3+} nanophosphors were prepared by high-temperature solid-state reaction. The raw materials include MgO, $SrCO_3$, SiO_2, Tb_2O_3 and they are all analytical reagents (AR). All raw materials were weighed, mixed, fully ground, and placed into a corundum crucible. The heating rate of the high-temperature furnace was set to be 20 °C/min and the reaction of mixture raw materials was kept for 180 min at 1300 °C in air environment. The stoichiometric ratio was chose to be $(1-0.05-x)Sr_2MgSi_2O_7$:xTb^{3+} ($x=0$, 0.2, 0.4, 0.6, 0.8, 1.0, 1.2, 1.4, 1.6, 1.8, 2.0, and 2.2 mol%) and the chemical reaction equation in the preparation process is

$$MgO + 2SrCO_3 + 2SiO_2 \rightarrow Sr_2MgSi_2O_7 + 2CO_2\uparrow. \quad (1)$$

Note that 5-mol% boric acid with a function of fusion agent was additionally mixed into the raw materials of every sample to make the reaction more thorough.

Figure 1 illustrates the x-ray diffraction patterns of $Sr_2MgSi_2O_7$:xTb^{3+} nanophosphors measured by XRD-6000 (Shimadzu Corporation, Japan). The radiation source is Cu $K\alpha 1$ and its wavelength is 0.154178 nm. The scan speed and scan range were set to be 2 °/min and 10°–80°, respectively. It can be found from Fig. 1 that the main diffraction peaks of synthesized $Sr_2MgSi_2O_7$ matrix powder are basically consistent with those in the standard card (PFD#75-1736). There were no new diffraction peaks appearing when Tb^{3+} ions were doped into the matrix. However, some diffraction peaks gradually weakened or even disappeared (*e.g.*, peaks at 31.34°, 39.46°, and 45.39°), whereas others (at 25.0°, 30.4°, 35.3°, and 44.1°) become stronger with the increase of Tb^{3+} concentration, implying that the incorporation of terbium ions improves the crystal quality of $Sr_2MgSi_2O_7$:Tb^{3+} nanophosphors.

The morphologies of $Sr_2MgSi_2O_7$:Tb^{3+} nanophosphors were characterized by SU8000 SEM (Hitachi, Japan), and the results are shown in Fig. 2. Figure 2(a) refers to the $Sr_2MgSi_2O_7$ matrix and figures 2(b)–2(d) show the nanophosphors doped with 0.6-, 1.0-, and 1.6-mol% terbium ions, respectively. It can be seen that the morphologies of nanoparticles are all spherical and the distributions of the particle sizes are shown in the insets of Fig. 2. It can be seen that there exist the gaps in Figs. 2(c) and 2(d) because the few particles are chosen in order to make the morphology of nanophosphor clearer and more visual. The average sizes in Figs. 2(a)–2(d) are different and they are 28, 46, 68, and 84 nm in turn, implying that the particle size of the nanophosphor gets larger with the Tb^{3+} doping concentration increasing. And the above result is consistent with XRD diffraction patterns according to the following Debye–Scherer formula[31]

$$D_{hkl} = \frac{k\lambda}{\beta\cos\theta}, \quad (2)$$

where D_{hkl} represents the grain diameter, k is the Scherer constant (about 0.89), λ, β, and θ denote the x-ray wavelength, the full width at half maximum (FWHM) of the diffraction peak, and the diffraction angle, respectively. It can be seen from Fig. 1 that the higher the doping concentration, the narrower the FWHM of the diffraction peak is. In other words, the β value becomes smaller with the Tb^{3+} concentration increasing and therefore the grain diameter D_{hkl} of $Sr_2MgSi_2O_7$:Tb^{3+} nanophosphor turns larger as indicated from Eq. (2).

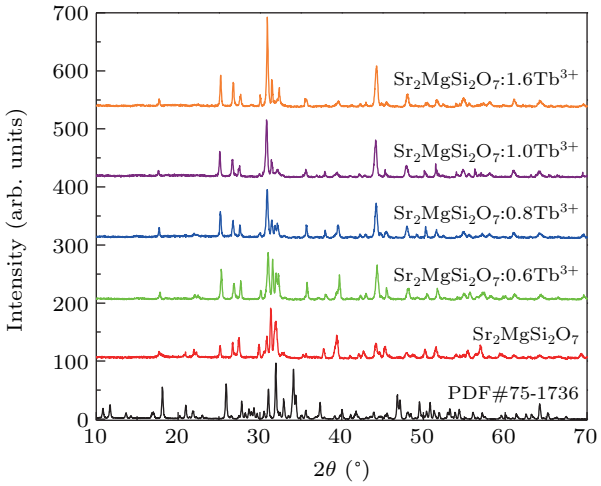


Fig. 1. XRD patterns of $Sr_2MgSi_2O_7$:Tb^{3+}.

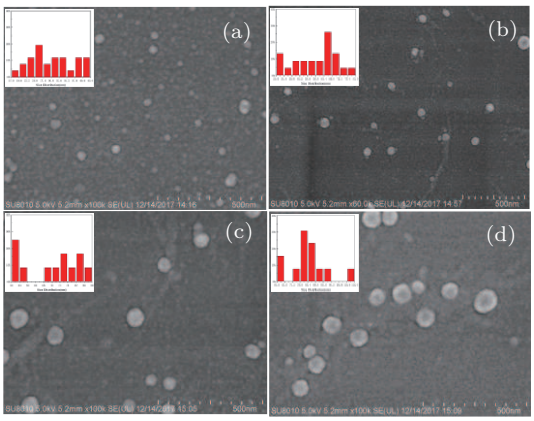


Fig. 2. SEM images of $Sr_2MgSi_2O_7$:Tb^{3+}.

3. Results and discussion

The excitation spectrum (green line) and emission spectra (fill area under curve with violet) of $Sr_2MgSi_2O_7$:1.6Tb^{3+} nanophosphor are measured using F4600 Fluorescence Spectrmeter (Hitachi, Japan), and the results are shown in Fig. 3.

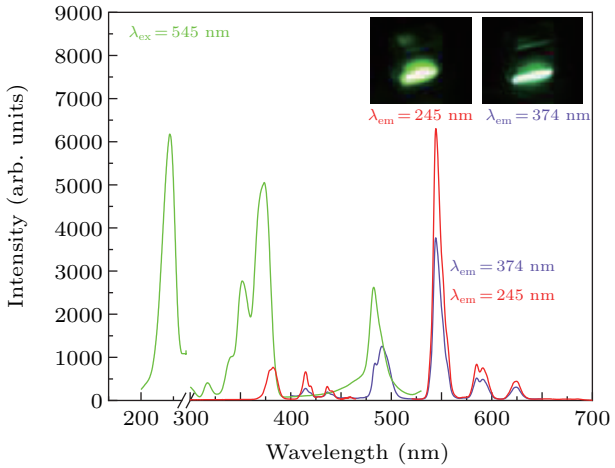


Fig. 3. Excitation and emission spectra of $Sr_2MgSi_2O_7$:1.6Tb^{3+} nanophosphor.

It can be found from Fig. 3 that there exist four intense excitation peaks at 245, 352, 374, and 483 nm, respectively, when the monitored wavelength is chosen to be 545 nm. What needs explaining is that the Break from 263 nm to 300 nm at the transverse axis is to avoid the influence of the harmonic wave generated from the monitored wavelength. Although the optimal excitation wavelength for obtaining the strongest green emission is 245 nm, the wavelength is in the deep ultraviolet region. It is known that the semiconductor chip of LED in DUV region is very expensive, and hence the price of LED product applying trivalent terbium as the active ion will be very high if 245 nm is selected as the excitation wavelength. Fortunately, for our $Sr_2MgSi_2O_7$:Tb^{3+} nanophosphor, the second-best excitation wavelength is 374 nm and, compared with DUV 245 nm, it extends for about 130 nm toward a long wavelength. Furthermore, the peak intensity at 374 nm is about 82% of that at 245 nm. Therefore, we can predict that the strong green emission from $Sr_2MgSi_2O_7$:Tb^{3+} nanophosphor can also be gained under 374-nm excitation. Especially, the cost of semiconductor chips of LED used as excitation sources will be lowered significantly.

We can also know from the emission spectra in Fig. 3 that there exist six PL peaks at 415, 437, 490, 545, 585, and 624 nm. All the center wavelengths of PL peaks are the same even under different excitations, but the intensities excited by 245 nm are more intense than those pumped by 374 nm, which coincides with the excitation spectrum in Fig. 3. The sketch map of levels and transitions of Tb^{3+} ion under 245-nm and 373-nm excitations, respectively, is shown in Fig. 4, and the peaks correspond respectively to transitions of Tb^{3+} ions $^5D_3 \rightarrow {}^7F_5$, $^5D_3 \rightarrow {}^7F_4$, $^5D_4 \rightarrow {}^7F_5$, $^5D_4 \rightarrow {}^7F_4$, $^5D_4 \rightarrow {}^7F_3$, and $^5D_4 \rightarrow {}^7F_2$. Thereinto, the green emission at 545 nm is the strongest, followed by the 490-nm blue emission. We need to emphasize here that the reason for the spectra at 490-nm and 585-nm bands to be split lies in the influence of the crystal field on Tb^{3+} ions, leading the energy levels of Tb^{3+} ions to be split.

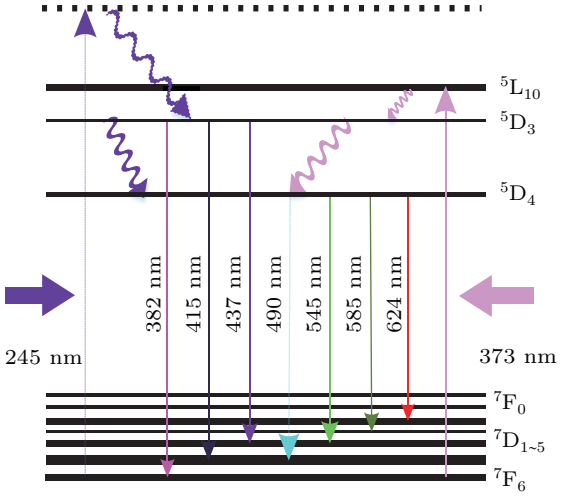


Fig. 4. Sketch map of levels and transitions of Tb^{3+} ion under 245-nm or 374-nm excitations nanophosphors.

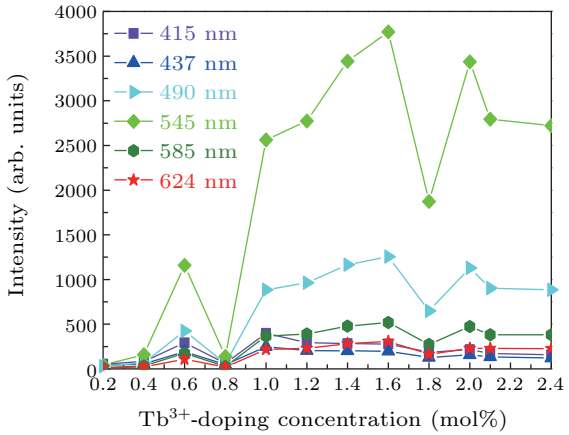


Fig. 5. Changes of PL intensities with varied Tb^{3+} doping concentration.

Photos in Fig. 3 demonstrate that the PL intensity of the $Sr_2MgSi_2O_7$:1.6Tb^{3+} nanophosphor pumped by 245 nm is a little stronger than that of the same sample pumped by 374 nm. Such a situation coincides with the measurement result of the excitation spectrum, *i.e.*, the excitation peak in DUV region is higher than that in NUV region. It should be noted that there are white-light areas in the photos. The main reason is that the emissions in those areas are too intense, resulting in the overexposure and saturation of the camera (Canon EOS 60D, Japan). In fact, the intense green emissions can still be observed by naked eyes from the so-called white-light areas in nanophosphor samples. Figure 5 shows that the PL intensities of all emission peaks vary with Tb^{3+} doping concentration and the optimal concentration is 1.6 mol%. It can also be seen from Fig. 5 and the inset of Fig. 6 that there exist clear fluctuations. The main reasons lie in some errors appear inevitably in the preparation and measurement process although

we try our best to ensure the uniformity in the experiments. on the other hand, the optimal Tb^{3+} concentrations in the various hosts may take different forms, that is, single peak or double peaks.[32,33] The two factors result in the fluctuations of curves as shown in Figs. 5 and 6.

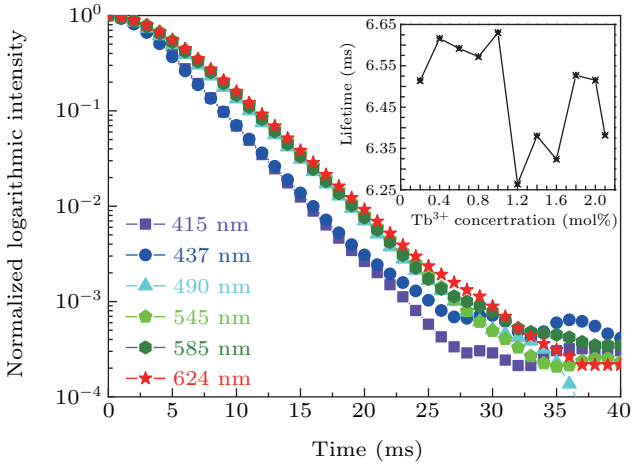


Fig. 6. Decay curves of different emissions of $Sr_2MgSi_2O_7$:Tb^{3+} nanophosphor.

Six decay curves corresponding to different spontaneous radiations of $Sr_2MgSi_2O_7$:1.6Tb^{3+} nanophosphor are shown in Fig. 6. It can be known that the decay rates of 415-nm and 437-nm emissions are obviously faster than those of 490, 545, 585, and 624 nm, indicating that the lifetime of $^5D_3$ energy level is shorter than that of $^5D_4$ energy level (see Fig. 4). After further fitting the decay curves of six emission peaks, it is found that they belong to biexponential decay functions, that is, $I = I_0 + A_1\exp(-t/\tau_1) + A_2\exp(-t/\tau_2)$, where $\tau_1 = [4.55, 4.44, 5.46, 5.78, 5.69, 5.89]$ ms and $\tau_2 = [5.35, 5.62, 6.54, 6.43, 6.37, 6.02]$ ms corresponding respectively to 415-, 437-, 490-, 545-, 585-, and 624-nm emission peaks. The inset in Fig. 6 shows changes of the lifetime corresponding to the 545-nm green emission of $Sr_2MgSi_2O_7$:xTb^{3+} nanophosphor with Tb^{3+} doping concentration and its range is in [6.24, 6.63] ms. For the $Sr_2MgSi_2O_7$:1.6Tb^{3+} nanophosphor with the optimal doping concentration, however, the value is not the longest but the second-shortest, which is worth investigating and exploring in depth in the future study.

According to Blasse theory,[34] the critical distance R_c for energy transfer can be expressed as the following formula:

$$R_c \approx 2\left[\frac{3V}{4\pi x_c Z}\right]^{1/3}, \tag{3}$$

where x_c denotes the critical concentration, V is the volume of unit cell, and Z refers to the number of chemical units in the unit cell. For $Sr_2MgSi_2O_7$:Tb^{3+} nanophosphor, $V = 0.402$ nm^3 and $Z = 2$, and thus $R_c = 0.602$ nm. Therefore, the nonradiative energy transfer among Tb^{3+} ions belongs to the electric multipole–electric multipole interaction because R_c is larger than the critical interaction distance $R_{c0} = 0.5$ nm. In other words, the electric multipole interaction will get stronger with the increase of the concentration, resulting in the decrease of PL intensity. Furthermore, the reason for the concentration quenching of $Sr_2MgSi_2O_7$:Tb^{3+} nanophosphor can be further analyzed based on Zhang's theory, that is, the relationship between the luminescent intensity I and the concentration x obeys the following expression:[35]

$$\frac{I}{x} = \frac{k}{1+\beta x^{S/3}} \approx k' x^{-S/3}, \tag{4}$$

where k and β are the constants, S is an electric multipole index and it represents the electric dipole–electric dipole interaction, the electric dipole–electric quadrupole interaction, and the electric quadrupole–electric quadrupole interaction for $S = 2$, 4, and 6, respectively. Considering $\beta x^{S/3} \gg 1$, equation (4) can be rewritten as a linear equation with dual logarithm coordinates. Figure 7 illustrates the $\lg(I/x) \sim \lg(x)$ fitting curve of 545-nm green emission under 374-nm excitation and the slope is about -1.847. Hence $S = 5.54$ is closer to 6, implying that the quenching mechanism of $Sr_2MgSi_2O_7$:Tb^{3+} nanophosphors is the electrical dipole–electric dipole interaction of the luminescent centers under 374-nm excitation.

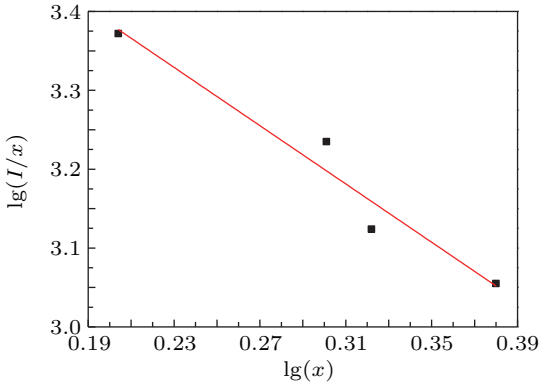


Fig. 7. The $\lg(I/x)$–$\lg(x)$ fitting curve of $Sr_2MgSi_2O_7$:Tb^{3+} phosphor.

4. Conclusion

In this work, a series of $Sr_2MgSi_2O_7$:Tb^{3+} nanophosphors is prepared by a high temperature solid-state reaction. The crystal structures and morphologies of representative samples are analyzed using XRD and SEM. And the results show that the main diffraction peaks of $Sr_2MgSi_2O_7$ matrix are basically consistent with those in the standard card, especially the crystal quality of $Sr_2MgSi_2O_7$:Tb^{3+} powder is improved through the incorporation of Tb^{3+} ions. It can be found from the SEM images that $Sr_2MgSi_2O_7$:Tb^{3+} nanoparticles possess all spherical structures and the average grain size becomes larger with the Tb^{3+} ion concentration increasing. The excitation spectrum shows that 374 nm is also an ideal excitation wavelength and the strong green emission at 545 nm is observed under 374-nm excitation. In addition, other PL peaks including 382, 415, 437, 490, 585, and 624 nm can also be

obtained at an optimal doping concentration of 1.6 mol%. The measurement results of decay curves indicate that the lifetime of $^5D_3$ energy level is shorter than that of $^5D_4$ energy level. The concentration quenching of the samples prepared in our work is because of the electrical dipole–electric dipole interaction of the luminescent centers.

References

[1] Shin S Y and Park S 2021 *J. Mater. Sci.* **32** 4311
[2] Shi J J, Liu B, Wang Q G, Tang H L, Wu F, Li D Z, Zhao H Y, Wang Z S, Deng W, Xu Z A, Xu J Y, Xu X D and Xu J 2018 *Chin. Phys. B* **27** 097801
[3] Wei Z T, Chen W B, Wang Z Q, Li N, Zhang P F, Zhang M G, Zhao L and Qiang Q P 2021 *J. Am. Ceram. Soc.* **104** 1750
[4] Hernández A G, Boyer D, Potdevin A, Chadeyon G, Murillo A G, Romo F C and Mahiou R 2017 *Opt. Mater.* **73** 350
[5] He W X, Du H L, Fu J, Luan F F, Li D W, Sun L Y and Guo D C 2021 *New J. Chem.* **45** 1446
[6] Wang Q, Qiu J B, Song Z G, Zhou D C and Xu X H 2014 *Chin. Phys. B* **23** 064211
[7] dos Santos J F M, Terra I A A, Astrath N G C, Guimarães F B, Baesso M L, Nunes L A O and Catunda T 2015 *J. Appl. Phys.* **117** 053102
[8] Gao X Y, Li C R, Li S F, Zhang H B, Li Z C, Hong Y Z and Sun J C 2017 *J. Lumin.* **190** 457
[9] Zhao L, Wang D Y, Wang Y H and Tao Y 2015 *J. Am. Ceram. Soc.* **97** 3913
[10] Bianchi G S, Zanuto V S, Astrath F B G, Malacarne L C, Terra I A A, Catunda T, Nunes L A O, Jacinto C, Andrade L H C, Lima S M, Baesso M L and Astrath N G C 2013 *Opt. Lett.* **38** 4667
[11] Nikifor R and Glauco S M 2017 *J. Lumin.* **190** 249
[12] Huang X Y, Li B and Guo H 2017 *J. Alloys Compd.* **695** 2773
[13] Alves L L S, de Lima R C, Schiavon M A, Gonçalves R R, Barbosa H P and Ferrari J L 2020 *J. Lumin.* **222** 117109
[14] Cui H, Zhu P F, Zhu H Y, Li H D and Cui Q L 2014 *Chin. Phys. B* **23** 057801
[15] Kumar D, Sharma M, Haranath D and Pandey O P 2017 *J. Alloys Compd.* **695** 726
[16] Yu H, Qi Y, Wu Y, Zhang J and Chen B 2016 *J. Nanosci. Nanotechno* **16** 3886
[17] Chen Y F, Bao Y, Yu Z P, Yang G C and Zhang L 2017 *J. Lumin.* **181** 71
[18] Barbara S S, Natalia P, Tomasz G, Maria Band Wojciech A P 2017 *J. Lumin.* **188** 400
[19] Srikanth K, Narsihma L, Narsimulu M, Kumar M S, Laxminarayana K and Srinivas M 2020 *AIP Conf. Proc.* **2269** 030058
[20] Bispo A G, Lima S A M, Lanfredi S, Praxedes F R and Pires A M 2019 *J. Lumin.* **214** 116604
[21] Jyothi K R, Bhagya K R, Nagabhushana H, Hegde V N, Murugendrappa M V, Prakash A P G, Daruka P B and Nagabhushana N M 2020 *Physica B* **590** 412195
[22] Igashira K, Nakauchi D, Ogawa T, Kato T, Kawaguchi N and Yanagida T 2020 *Opt. Mater.* **109** 110270
[23] Homayoni H, Ma L, Zhang J, Sahi S K, Rashidi L H, Bui B and Chen W 2016 *Photodiagn. Photodyn. Ther.* **16** 90
[24] Hai O, Ren Q, Wu X L, Zhang Q, Zhang Z H and Zhang Z Z 2019 *J. Alloys Compd.* **779** 892
[25] Tshabalala M A, Swart H C, Dejene F B, Coetsee E and Ntwaeaborwa O M 2016 *Appl. Surf. Sci.* **360** 409
[26] Sahu I P 2016 *Appl. Phys. A* **122** 855
[27] Wang Y, Chen Y, Sun Q and Yan B 2017 *J. Mater. Res.* **32** 547
[28] Yuan B, Song Y H, Kong L, Dai C B and Zou H F 2018 *Physica B* **550** 75
[29] He L, Jia B L, Che L Y, Li W S and Sun W M 2016 *J. Lumin.* **172** 317
[30] Liu X, Zhang X X and Zhou Z F 2016 *Mater. Res. Bull.* **79** 84
[31] Pathak C S, Mishra D D, Agarwala V and Mandal M N 2012 *Ceram. Int.* **38** 6191
[32] Vikas D, Raunak K T, Rituraj C and Vijay S 2021 *Optik.* **226** 165926
[33] Bhuneshwar V, Baghel R N, Bisen D P, Brahme N and Khare A 2020 *J. Alloys Compd.* **838** 155326
[34] Blasse G 1968 *Phys. Lett. A* **28** 444
[35] Zhang J Y, Zhuang W D, Xing X R, Liu R H, Chen G T, Liu Y H and Chen L 2014 *Mater. Lett.* **131** 248